tvst

https://doi.org/10.1167/tvst.7.5.13

Article

Comparison of Green Versus Blue Fundus Autofluorescence in *ABCA4*-Related Retinopathy

Philipp L. Müller[1,2], Maximilian Pfau[1], Matthias M. Mauschitz[1], Philipp T. Möller[1], Johannes Birtel[1,2], Petrus Chang[1], Martin Gliem[1–3], Steffen Schmitz-Valckenberg[1], Monika Fleckenstein[1], Frank G. Holz[1,2], and Philipp Herrmann[1,2]

[1] Department of Ophthalmology, University of Bonn, Bonn, Germany
[2] Center for Rare Diseases, University of Bonn, Bonn, Germany
[3] Oxford Eye Hospital, Oxford University Hospitals NHS Foundation Trust, Oxford, UK

Correspondence: Philipp L. Müller, University of Bonn, Department of Ophthalmology, Ernst-Abbe-Str. 2, D-53127 Bonn, Germany. e-mail: Philipp.Mueller@ukbonn.de

Received: 29 March 2018
Accepted: 24 July 2018
Published: 1 October 2018

Keywords: Stargardt disease; retina; retinal pigment epithelium; atrophy; interreader correlation

Citation: Müller PL, Pfau M, Mauschitz MM, Möller PT, Birtel J, Chang P, Gliem M, Schmitz-Valckenberg S, Fleckenstein M, Holz FG, Herrmann P. Comparison of green versus blue fundus autofluorescence in *ABCA4*-related retinopathy. Trans Vis Sci Tech. 2018;7(5):13, https://doi.org/10.1167/tvst.7.5.13

Purpose: To investigate the interreader and intermodality agreement for grading of retinal pigment epithelium (RPE) atrophy lesion size in *ABCA4*-related retinopathy using green (GAF) and blue fundus autofluorescence (BAF) imaging.

Methods: In this cross-sectional case series, 97 eyes of 49 patients with RPE atrophy secondary to *ABCA4*-related retinopathy underwent GAF- (518 nm excitation light) and BAF- (488 nm excitation light) imaging using confocal scanning laser ophthalmoscopy (Spectralis HRA, Heidelberg Engineering, Heidelberg, Germany). Lesions with definitely decreased autofluorescence (DDAF) and questionably decreased autofluorescence (QDAF) in GAF and BAF imaging were analyzed separately by five independent readers using semiautomated software (RegionFinder, Heidelberg Engineering). Intermodality and interreader agreements were assessed for the square-root lesion size, lesion perimeter, and circularity.

Results: GAF- and BAF-based measurements of DDAF and QDAF showed high intermodality and interreader agreement concerning square-root lesion size, as well as shape descriptive parameters (perimeter and circularity). Interreader agreement of square-root lesion size was slightly, hence not significantly higher for GAF-based grading ([95% coefficients of repeatability, intraclass correlation coefficient] DDAF: 0.215 mm, 0.997; QDAF: 0.712 mm, 0.981) compared to BAF-based grading (DDAF: 0.232 mm, 0.997; QDAF: 0.764 mm, 0.978). However, DDAF-measurements revealed distinctly more reproducible results than QDAF-measurements. Foveal sparing did not interfere with intermodality agreement.

Conclusions: Both GAF- and BAF-based quantification of RPE atrophy showed very reliable results with possible superiority of GAF in the context of less energetic excitation light.

Translational Relevance: The high interreader agreement qualifies the use of DDAF progression in GAF and BAF imaging as potential morphologic outcome measure for interventional clinical trials and disease monitoring.

Introduction

ABCA4-related retinopathy (Online Mendelian Inheritance in Man # 601691) is among the most frequent causes for retinal dystrophy-related loss of vision in the working age.[1–4] The disease is caused by biallelic mutations in the *ATP-binding cassette subfamily A member 4 (ABCA4)* gene, that leads to dysfunction of the encoded protein product (ABCA4).[5,6] Subsequently, excessive amounts of lipofuscin accumulate in the lysosomal compartment of retinal pigment epithelium (RPE) cells, which has been shown to exert toxic effects on the RPE and photoreceptors leading to RPE atrophy.[5–7]

RPE lipofuscin contains multiple molecular constituents with autofluorescent properties that can be

visualized with fundus autofluorescence (AF) imaging using blue excitation light (BAF, 488 nm).[8–10] Thus, *ABCA4*-related retinopathy is characterized by an overall increased BAF intensity[11,12] that contrasts with hypoautofluorescent areas of RPE atrophy allowing semiautomated quantification of atrophic areas.[13–15] Quantification of atrophic areas might be of interest as a clinical endpoint for interventional clinical trials as already established in geographic atrophy secondary to age-related macular degeneration (AMD).[16] Recently, shape descriptive parameters such as lesion perimeter and circularity have been proposed as prognostic biomarkers for AMD in this context.[17]

The progression rate of RPE atrophy in *ABCA4*-related retinopathy has been reported to be slower compared to AMD.[15,18,19] Furthermore, the identification of RPE atrophy in *ABCA4*-related retinopathy appears to be more challenging as it encompasses variable stages toward complete atrophy ranging from questionable (QDAF) to definitely (DDAF) decreased AF.[20,21] A previous study correlated OCT-findings in QDAF and DDAF and found significantly thinner outer retinal layers (outer nuclear layer and combined layers between external limiting membrane and Bruch's membrane) in the latter case, considering QDAF as a transition state between healthy retina and DDAF.[22] As both RPE atrophy manifestations may be present within the same eye, more sophisticated measurement approaches are required.[20,21]

An innovative AF imaging modality has been proposed, using green excitation light (GAF, 518 nm) that lies outside the absorption maximum of the macular pigment.[23,24] Since macular pigment (lutein, zeaxanthin, and meso-zeaxanthin) absorbs short-wavelength excitation light, the evaluation of the fovea in BAF imaging is challenging.[24–26] Hence, GAF imaging may be more accurate in the determination of small, central lesions including the differentiation between foveal involvement and foveal sparing. Furthermore, ex vivo data suggest that green-light compared to blue-light illumination may reduce lipofuscin mediated light-induced retinal toxicity—a concern given that *ABCA4*-related retinopathy represents the prototypical lipofuscin accumulation disease.[27–29]

However, advantages of GAF-based grading, including higher patient comfort due to excitation light with lower energy, have only been shown for AMD in two recent studies.[17,25] To date, comparisons of GAF and BAF imaging concerning the evaluation of RPE atrophy secondary to *ABCA4*-related retinopathy have not been carried out. In the view of future therapeutic clinical trials in this field, valid and reliable biomarkers are mandatory.[30–33]

Herein, we investigated the interreader and intermodality agreement for semiautomated grading of RPE atrophy secondary to *ABCA4*-related retinopathy using GAF and BAF imaging. We tested the hypothesis that there are no differences in lesion size, perimeter, and circularity measurements as well as the interreader correlation among both assessed AF modalities.

Methods

This monocenter cross-sectional case series was performed at the Department of Ophthalmology of the University of Bonn, Germany. The study was in adherence with the Declaration of Helsinki. Institutional Review Board approval (Institutional Review Board of the University of Bonn, Germany; ethics approval ID 316/11 and 288/17) and patients' informed consent were obtained.

Patients with *ABCA4*-related retinopathy were defined by the presence of at least one disease causing mutation in *ABCA4* in Sanger sequencing with multiplex ligation-dependent probe amplification analysis or next-generation sequencing[34] and a phenotype consistent with *ABCA4*-related retinopathy,[30] and were recruited from the retinal dystrophy clinic at the Department of Ophthalmology, University of Bonn, Germany. In accordance to previous reports, RPE-atrophy was defined as "DDAF" in case of demarcated lesions with ≥90% darkness or as "QDAF" in case of demarcated lesions with 50% to 90% darkness (optic disk served as reference with 100% darkness).[20,35] Minimum lesion size was defined as 0.05 mm^2 (each single atrophic area in cases of multifocality).[14,16,20,36] Exclusion criteria contained insufficient pupil dilation, additional retinal pathology, previous vitreoretinal surgery, or other ocular comorbidities substantially affecting visual function and/or imaging quality.

Imaging

All patients underwent a complete ophthalmologic examination. Prior to imaging, pupils were dilated using 0.5% tropicamide and 2.5% phenylephrine to at least 7 mm diameter. The imaging protocol consisted of simultaneous BAF (488 nm excitation) and GAF

(518 nm excitation) imaging using confocal scanning laser ophthalmoscopy (cSLO; Spectralis HRA, Heidelberg Engineering, Heidelberg, Germany). An emission spectrum of 530 to 720 nm was used and the field of view was set to 30° × 30° (centered on the fovea). Within the manufacturer's software, a minimum of 16 frames per image were automatically aligned and averaged to optimize the signal-to-noise ratio.

Image Processing

Measurements of RPE atrophy lesions in GAF and BAF images were performed by five experienced masked readers (PLM, MMM, PTM, JB, and PC), using the semiautomated RegionFinder software (Heidelberg Engineering, version 2.6.3), which has been previously validated for quantification of RPE atrophy in AMD.[14] Briefly, the grading task was carried out on separate days and in random order. The readers set at least one seeding point inside of each atrophic region with DDAF by selecting the pixel with the lowest FAF signal (darkest gray value). Subsequently, the growth power for each seeding point was increased resulting in the inclusion of adjacent pixels depending on the gray value, until the delineation just exceeded the boundaries of the DDAF. Finally, the growth power had to be decreased by one increment below this threshold.[14] The growth limit function was used if the segmentation algorithm included the edges of the image frame and retinal vessels or macula pigment were excluded from the measured lesion area through the automated "vessel detection," "shadow correction," or by placing manual constraints, respectively. Interreader variability may be introduced at each of these steps. After saving of the grading results for DDAF, all DDAF lesions were transferred to constraints in order to quantify atrophic regions with QDAF in the same manner (Fig. 1).

Compared to RPE atrophy lesion size, shape descriptive factors may be more susceptible to small differences of the actual underlying delineations, as has been shown for AMD.[17] Therefore, the exported images were transferred to ImageJ (Bethesda, MD) to measure the (cumulative) lesion circularity and (cumulative) lesion perimeter using a custom-built plug-in as previously described.[17,37] Further, eyes were classified into foveal involvement or noninvolvement, according to the extent of RPE atrophy in/near the fovea.[23]

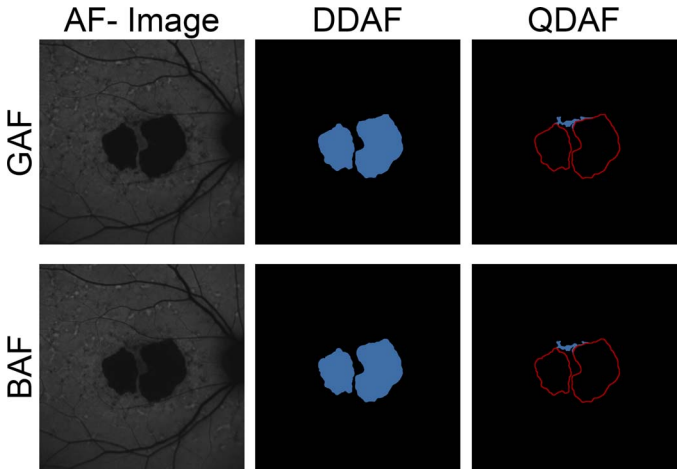

Figure 1. Grading of GAF and BAF images. Measurements of DDAF to QDAF decreased AF (≥90% darkness and 50%–90% darkness, respectively) were performed semiautomatically based on GAF (*top*) and BAF (*bottom*) images. In a first step, DDAF (*blue area*, *middle*) was annotated based on gray levels. Then, DDAF delineations were transferred to constraints (*red lines*, *right*) in order to measure QDAF (*blue area*, *right*). Despite absorption due to macular pigment, the high AF intensity in *ABCA4*-related retinopathy usually allows distinct demarcation and validation of foveal involvement.

Electroretinogram

Electroretinogram (ERG) was performed in accordance to ISCEV standards using a Ganzfeld stimulator and Burian–Allen bipolar corneal electrodes (Toennies Multiliner Vision 1.70, Hochberg, Germany). Based on full-field ERG, patients can be categorized according to the classification developed by Lois et al.[38]: group 1 contained eyes with normal responses on scotopic and photopic full-field ERG, group 2 eyes with normal scotopic responses but reduced (over 2 standard deviations) photopic B-wave and 30-Hz flicker amplitudes, and group 3 eyes with ERG reductions involving both rod- and cone-driven responses. Previously published data had shown the prognostic value of this ERG-based classification for disease progression.[18,38,39]

Statistical Analysis

Statistical analysis was performed using the software environment R (version 3.2.3, The R Foundation for Statistical Computing, Vienna, Austria)[40] similar to previous published data.[17] Briefly, area measurements were square-root transformed to obtain normally distributed data. Further, square-root transformed RPE atrophy lesion size has previously been suggested as clinical endpoint for upcoming clinical trials concerning macular degener-

ation in order to reduce the dependence of growth rates on baseline lesion size.[41,42] Mixed-effects models considering imaging modality as fixed effect (GAF versus BAF) and visit as well as reader as random effects were used for the analyses. Significance of the imaging modality was determined using likelihood ratio tests comparing a reduced model (without the fixed effect) with the full model. Intraclass correlation coefficients (ICCs; two-way random, absolute agreement), 95% coefficients of repeatability (CRs), and coefficients of variation (CVs) were determined for lesion size, perimeter, as well as the circularity in both AF modalities.[43,44] Bland-Altman plots were generated for visualization of limits of agreement. Spearman's rank correlation coefficients (ρ) were calculated between the absolute differences among measurements and the mean values to determine whether measurement variability increases with lesion size.[44]

Results

Cohort Characteristics

We included both eyes of 48 patients and only one eye (OD) of one patient due to history of total rhegmatogenous retinal detachment in the left eye. The mean age was 39.1 ± 19.3 years (±SD; range, 9–86 years; 33 women). RPE atrophy was present in all 97 eyes. Hereof, seven eyes showed only DDAF, 40 eyes only QDAF, and 50 eyes both DDAF and QDAF. Foveal noninvolving RPE atrophy was present in 21 eyes, mostly present in patients with late-onset (≥45 years) of first reported symptoms (14 of 21 eyes). Forty eyes were assigned to full-field ERG-based group 1, 37 eyes to group 2, and 20 eyes to group 3 (Table 1). Forty-five patients were found to have two disease-causing mutations. Three patients only revealed one disease-causing mutation but showed a phenotype consistent with *ABCA4*-related retinopathy.[30]

Table 1. Demographic and Clinical Data of All Included Patients and Eyes

Eyes (patients)	97 (49)
Mean age ± SD (range) in years	39.4 ± 19.2 (9–86)
Sex, *n* (%)	
Male	15 (31.3)
Female	33 (68.7)
Lens status, *n* (%)	
Phakic	90 (92.8)
Pseudophakic	7 (7.2)
ERG-based classification, *n* (%)	
Group 1	40 (41.2)
Group 2	37 (38.1)
Group 3	20 (20.6)
RPE atrophy	
DDAF, *n* (%)	57 (58.8)
QDAF *n* (%)	90 (92.8)
Foveal involvement, *n* (%)	
Foveal atrophy	75 (77.3)
Extrafoveal atrophy	22 (22.7)
Thereof foveal sparing[a]	14 (14.4)

[a] Foveal sparing was defined as an intact, residual foveal island being surrounded by more than 270° of DDAF areas.[15]

RPE Atrophy Lesion Size: Intermodality Agreement

Both AF modalities (GAF and BAF) did not reveal any significant difference concerning DDAF and QDAF lesion size (Table 2). In fact, the overall mean square-root DDAF and QDAF lesion size in GAF images was only slightly larger compared to BAF-based measurements (0.004 and 0.009 mm, respectively).

To evaluate individual (eye) measurement variability between both AF modalities, the limits of agreement (highlighted as dashed lines in the Bland-Altman plots; Fig. 2) were investigated. Limits of agreement were more narrow for DDAF (–0.106 to 0.114 mm) compared to QDAF (–0.235 to 0.252 mm), indicating higher individual (eye) intermodality agreement in DDAF measurements. However, the variability increased with larger DDAF ($\rho = 0.478$, $P < 0.001$) and QDAF ($\rho = 0.605$, $P < 0.001$) lesion sizes according to Spearman's rank correlation coefficient (ρ) for absolute differences and mean values.

In line with these findings, eyes assigned to ERG-based group 3 (i.e., widespread disease manifestation consistent with presence of large amounts of hypo-autofluorescent flecks in our cohort; Table 2, Fig. 3) showed the least intermodality agreement (Fig. 2): In DDAF lesion size measurements, the limits of agreement (mean differences) were wider in group 3 with –0.166 to 0.205 mm (0.019 mm) compared to group 2 with –0.050 to 0.044 mm (–0.003 mm) and group 1 with –0.018 to 0.011 mm (–0.003 mm). This effect was even more obvious in QDAF lesion size measurements with limits of agreement (mean differences) of –0.390 to 0.525 mm (0.068 mm) for group 3, –0.191 to 0.149 mm (0.021 mm) for group 2, and –0.101 to 0.114 mm (–0.006 mm) for group 1.

Table 2. Intermodality Agreement in Dependence on Included Eyes and Subgroups

Group Grading Modality	GAF, Mean ± SD	BAF, Mean ± SD	$\chi^2(1)$	*P* Value[a]
All eyes ($n = 97$)				
DDAF ($n = 57$)				
Square-root lesion size [mm]	2.874 ± 1.551	2.870 ± 1.546	0.319	0.572
Perimeter [mm]	22.368 ± 24.316	22.202 ± 24.096	1.709	0.191
Circularity [AU]	0.418 ± 0.264	0.420 ± 0.264	0.288	0.591
QDAF ($n = 90$)				
Square-root lesion size [mm]	2.325 ± 1.855	2.316 ± 1.824	0.251	0.616
Perimeter [mm]	55.254 ± 74.452	54.686 ± 72.982	0.458	0.499
Circularity [AU]	0.245 ± 0.283	0.242 ± 0.277	0.344	0.557
Group 1 ($n = 40$)				
DDAF ($n = 9$)				
Square-root lesion size [mm]	1.504 ± 0.737	1.507 ± 0.735	0.239	0.625
Perimeter [mm]	6.535 ± 3.410	6.495 ± 3.397	1.032	0.310
Circularity [AU]	0.722 ± 0194	0.735 ± 0.191	1.490	0.222
QDAF ($n = 39$)				
Square-root lesion size [mm]	1.148 ± 0.619	1.142 ± 0.619	0.392	0.531
Perimeter [mm]	11.036 ± 11.442	10.867 ± 11.039	0.768	0.381
Circularity [AU]	0.419 ± 0.296	0.409 ± 0.285	0.957	0.328
Group 2 ($n = 37$)				
DDAF ($n = 30$)				
Square-root lesion size [mm]	2.655 ± 1.422	2.658 ± 1.425	0.291	0.589
Perimeter [mm]	16.239 ± 10.163	16.169 ± 10.003	0.561	0.454
Circularity [AU]	0.458 ± 0.232	0.457 ± 0.228	0.072	0.788
QDAF ($n = 33$)				
Square-root lesion size [mm]	2.158 ± 1.171	2.179 ± 1.202	0.638	0.425
Perimeter [mm]	44.898 ± 45.848	45.676 ± 46.380	0.755	0.385
Circularity [AU]	0.152 ± 0.213	0.148 ± 0.216	0.355	0.551
Group 3 ($n = 20$)				
DDAF ($n = 18$)				
Square-root lesion size [mm]	3.924 ± 1.406	3.905 ± 1.399	0.980	0.322
Perimeter [mm]	40.500 ± 34.913	40.111 ± 34.672	1.067	0.302
Circularity [AU]	0.200 ± 0.133	0.200 ± 0.129	0.015	0.969
QDAF ($n = 28$)				
Square-root lesion size [mm]	5.179 ± 1.647	5.111 ± 1.539	0.991	0.320
Perimeter [mm]	170.043 ± 78.266	166.147 ± 76.466	1.040	0.308
Circularity [AU]	0.038 ± 0.072	0.051 ± 0.122	3.667	0.056

[a] *P* values were obtained using likelihood ratio tests.

Shape Descriptive Factors: Intermodality Agreement

Despite being more susceptible to small differences of the underlying delineation, both AF modalities did not reveal any significant differences concerning DDAF perimeter, QDAF perimeter, DDAF circularity, and QDAF circularity with a mean difference of 0.163, 0.567, −0.002, and 0.003 mm, respectively (Table 2).

Individual (eye) intermodality agreement was again investigated by limits of agreement in the Bland-Altman plots (Fig. 2): Concerning perimeter measurements, the limits of agreement (GAF versus BAF) were distinctly narrower for DDAF (−0.782 to 1.107 mm) than for QDAF (−8.211 to 9.345 mm), as

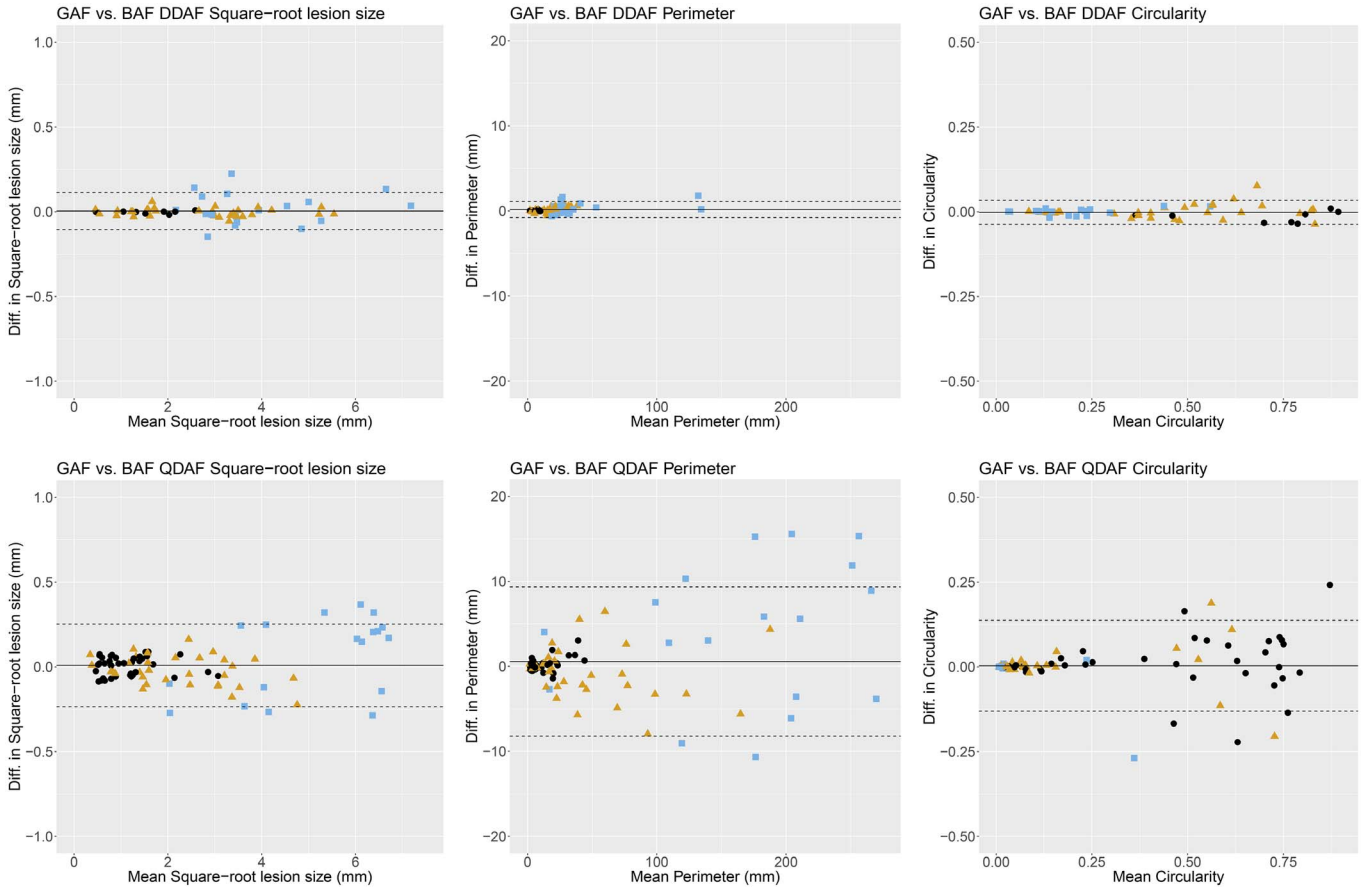

Figure 2. Intermodality agreement. The Bland-Altman plots demonstrate the intermodality agreement of both AF modalities (GAF versus BAF) concerning DDAF (*top*) as well as QDAF (*bottom*) square-root lesion size (*left*), perimeter (*middle*), and circularity (*right*) separated for ERG-based group classification[38] (group 1, *black dots*; group 2, *yellow triangles*; group 3, *blue squares*). The *solid line* indicates the mean difference and the *dashed lines* indicate the 95% limits of agreement. Overall, GAF- and BAF-based gradings showed similar results. However, DDAF measurements revealed higher levels of agreement compared to QDAF.

has been described above for the lesion size measurements. Of note, perimeter measurements had higher values and therefore higher absolute variability (Table 2). In this context, eyes with higher perimeter values (i.e., due to multifocal hypofluorescent flecks especially in groups 2 and 3; Fig. 3) also showed more pronounced individual variability ($\rho = 0.697$, $P < 0.001$ and $\rho = 0.834$, $P < 0.001$ for DDAF and QDAF perimeter, respectively). In DDAF perimeter measurements, the limits of agreement (mean differences) were wider in group 3 with −1.949 to 1.806 mm (0.378 mm) and group 2 with −0.530 to 0.671 mm (0.070 mm) compared to group 1 with −0.090 to 0.170 (0.040 mm). In QDAF perimeter, the effect was even more pronounced as limits of agreement (mean differences) ranges −12.468 to 20.259 mm (3.896 mm) for group 3, −6.902 to 5.346 mm (−0.778 mm) for group 2 and −1.343 to 1.681 (0.169 mm) for group 1 (Fig. 2).

The circularity calculations of the GAF- and BAF-based grading data did not reveal any significant differences (Table 2). Despite higher circularity values, the limits of agreement (GAF versus BAF) were narrower for DDAF (−0.037 to 0.034) compared to QDAF (−0.131 to 0.137), indicating easier demarcation of DDAF lesions. In this context, highest DDAF and QDAF circularity was calculated in group 1 eyes that usually showed a single lesion restricted to central fovea, and lowest circularity was found in group 3 eyes with highest amounts of multifocal hypofluorescent flecks in our cohort, likewise in both AF modalities (Fig. 2, Table 2).

RPE Atrophy Lesion Size: Interreader Agreement

The CR (i.e., the value below which the difference between two measurements will lie with a probability

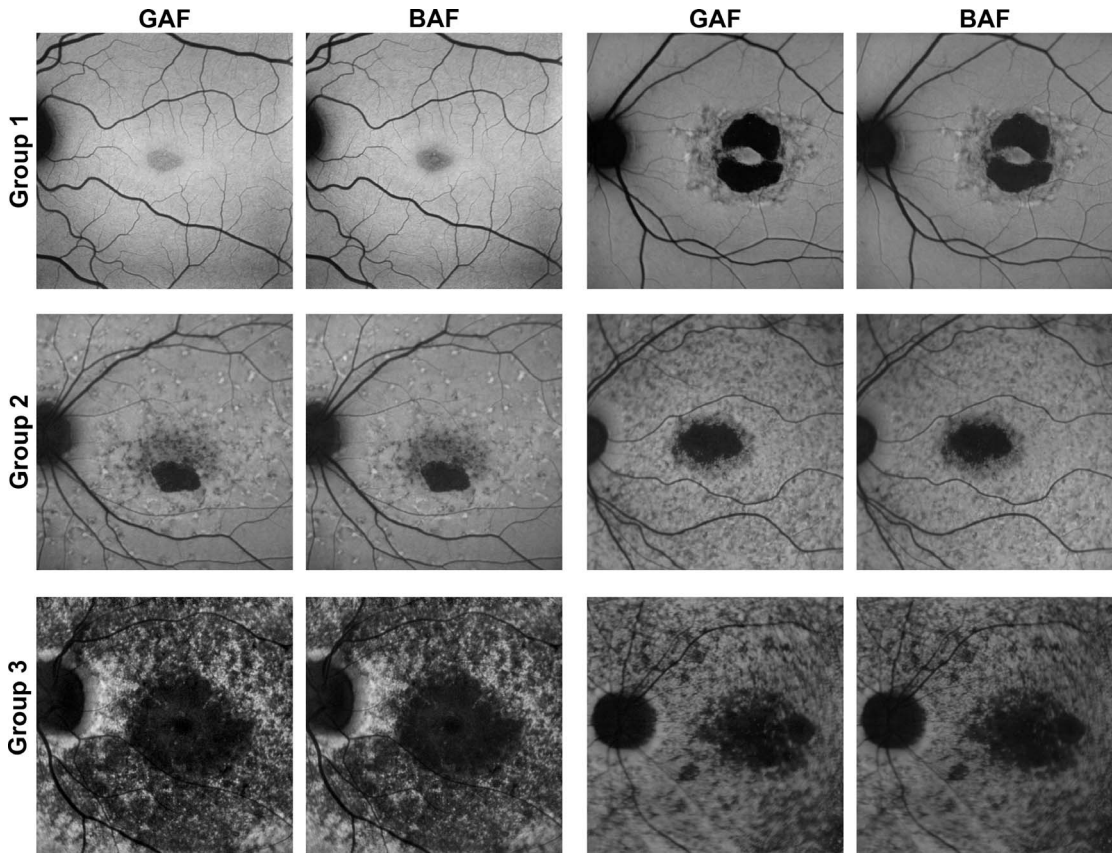

Figure 3. Exemplary images of eyes separated by ERG-based classification. Two exemplary eyes of each ERG-based group[38] are presented to demonstrate the high variability of *ABCA4*-related retinopathy and therefore different levels of interreader and intermodality agreement. The phenotypic spectrum of group 1 eyes ranges from eyes with only a central area of QDAF to eyes with DDAF surrounded by QDAF or flecks. Group 2 eyes typically revealed one or multiple well-circumscribed areas of DDAF with multiple hypo-and hyperautofluorescent flecks up to/over the vascular arcades. Group 3 usually contains eyes with multiple widespread hypoautofluorescent areas. Of note, images of both AF modalities differ only slightly, most obviously in the very mild phenotype of the first group 1 eye (*top left*).

of 0.95), CV and ICC indicated that the square-root DDAF lesion size grading had excellent interreader agreement, with slightly more congruent results in GAF images (Table 3; Supplementary Fig. 1). Despite the fact that CV and ICC take the underlying bigger QDAF lesion size into account, the square-root QDAF lesion size measurements showed lower interreader agreement compared to DDAF. This may indicate less reliable QDAF measurements. Nevertheless, the GAF- and BAF-based QDAF lesion size grading interreader agreement was overall still excellent (Table 3; Supplementary Fig. 1).

Each subgroup revealed excellent interreader agreement concerning DDAF and QDAF lesion size measurements, without relevant differences between both AF-modalities despite a consistent trend toward more congruent results for GAF-based measurements. Nevertheless, group 3 eyes revealed slightly lower interreader agreement—in particular for the CR and ICC of QDAF lesion size grading—compared to groups 1 and 2, most likely due to the challenging demarcation of the multifocal hypoautofluorescent flecks and atrophic areas that are typically found in these eyes (Fig. 3, Table 3).

Shape Descriptive Factors: Interreader Agreement

Equivalent to lesion size, interreader agreement for RPE atrophy lesion perimeter and lesion circularity were analyzed. The DDAF-based CR, CV, and ICC for both shape descriptive factors were excellent overall and for each subgroup (Table 3). In contrast, the partially challenging demarcation of many QDAF areas also revealed distinctly lower interreader agreement for perimeter and circularity, especially for group 3 eyes with widespread disease manifestation. The overall slightly higher interreader agreement for

Table 3. Interreader Agreement in Dependence on Included Eyes and Subgroups

Group Grading Modality	AF Modality	CR	CV [%]	ICC (95% CI)
All eyes ($n = 97$)				
DDAF ($n = 57$)				
Square-root lesion size	GAF	0.215 mm	2.70	0.997 (0.996–0.998)
	BAF	0.232 mm	2.92	0.997 (0.995–0.998)
Perimeter	GAF	4.203 mm	6.78	0.996 (0.994–0.998)
	BAF	4.382 mm	7.12	0.996 (0.994–0.997)
Circularity	GAF	0.104	8.94	0.980 (0.971–0.987)
	BAF	0.107	9.22	0.979 (0.969–0.986)
QDAF ($n = 90$)				
Square-root lesion size	GAF	0.712 mm	11.05	0.981 (0.974–0.987)
	BAF	0.764 mm	11.90	0.978 (0.970–0.984)
Perimeter	GAF	36.353 mm	23.73	0.970 (0.959–0.978)
	BAF	36.141 mm	23.84	0.969 (0.958–0.978)
Circularity	GAF	0.215	31.61	0.929 (0.905–0.949)
	BAF	0.222	33.08	0.922 (0.896–0.944)
Group 1 ($n = 40$)				
DDAF ($n = 9$)				
Square-root lesion size	GAF	0.111 mm	2.66	0.997 (0.992–0.999)
	BAF	0.100 mm	2.39	0.998 (0.994–0.999)
Perimeter	GAF	0.554 mm	3.06	0.996 (0.990–0.999)
	BAF	0.554 mm	3.08	0.997 (0.992–0.999)
Circularity	GAF	0.148	7.42	0.928 (0.830–0.980)
	BAF	0.163	7.98	0.912 (0.797–0.976)
QDAF ($n = 39$)				
Square-root lesion size	GAF	0.277 mm	8.72	0.974 (0.959–0.985)
	BAF	0.300 mm	9.48	0.970 (0.953–0.983)
Perimeter	GAF	5.613 mm	18.35	0.970 (0.951–0.983)
	BAF	5.681 mm	18.86	0.967 (0.947–0.980)
Circularity	GAF	0.296	25.47	0.882 (0.820–0.929)
	BAF	0.288	25.43	0.880 (0.819–0.928)
Group 2 ($n = 37$)				
DDAF ($n = 30$)				
Square-root lesion size	GAF	0.124 mm	1.68	0.999 (0.998–0.999)
	BAF	0.152 mm	2.06	0.998 (0.997–0.999)
Perimeter	GAF	1.753 mm	3.89	0.996 (0.993–0.998)
	BAF	1.753 mm	3.91	0.996 (0.993–0.998)
Circularity	GAF	0.096	7.53	0.978 (0.963–0.988)
	BAF	0.097	7.64	0.977 (0.961–0.988)
QDAF ($n = 33$)				
Square-root lesion size	GAF	0.650 mm	10.87	0.961 (0.936–0.978)
	BAF	0.722 mm	11.97	0.955 (0.926–0.975)
Perimeter	GAF	23.356 mm	18.77	0.967 (0.946–0.982)
	BAF	23.683 mm	18.71	0.967 (0.946–0.982)
Circularity	GAF	0.135	31.97	0.950 (0.919–0.972)
	BAF	0.166	40.38	0.928 (0.884–0.959)

Table 3. Continued

Group Grading Modality	AF Modality	CR	CV [%]	ICC (95% CI)
Group 3 ($n = 20$)				
DDAF ($n = 18$)				
Square-root lesion size	GAF	0.351 mm	3.22	0.992 (0.984–0.997)
	BAF	0.361 mm	3.33	0.991 (0.983–0.996)
Perimeter	GAF	7.333 mm	6.53	0.995 (0.989–0.998)
	BAF	7.333 mm	6.59	0.994 (0.988–0.997)
Circularity	GAF	0.089	16.22	0.944 (0.894–0.976)
	BAF	0.087	15.73	0.943 (0.893–0.975)
QDAF ($n = 28$)				
Square-root lesion size	GAF	1.264 mm	8.81	0.928 (0.865–0.968)
	BAF	1.326 mm	9.36	0.910 (0.835–0.960)
Perimeter	GAF	74.532 mm	15.81	0.892 (0.803–0.952)
	BAF	73.806 mm	16.03	0.889 (0.799–0.951)
Circularity	GAF	0.081	76.82	0.857 (0.746–0.935)
	BAF	0.124	86.67	0.878 (0.780–0.945)

GAF-based measurements of shape descriptive factors was not significant and even inconsistent in the different subgroups (e.g., QDAF circularity in group 3 showed higher ICC in BAF-based grading; Table 3).

Foveal Noninvolvement: Intermodality and Interreader Agreement

Recent AMD studies showed that highest disagreement between readers and variations between both AF-modalities are present in eyes with foveal noninvolvement. It was concluded that the differences most likely derived from the difficult assessment of foveal involvement of RPE atrophy secondary to AMD in BAF-based images.[17,25] Therefore, an additional subgroup analysis concerning the eyes with foveal noninvolvement was conducted in this study; however, there were no significant differences in this phenotypical subgroup between both AF-modalities concerning DDAF lesion size ([likelihood ratio test] $\chi^2(1) = 1.228$, $P = 0.268$), QDAF lesion size ($\chi^2(1) = 0.101$, $P = 0.751$), DDAF perimeter ($\chi^2(1) = 2.107$, $P = 0.147$), QDAF perimeter ($\chi^2(1) = 0.332$, $P = 0.565$), DDAF circularity ($\chi^2(1) = 3.162$, $P = 0.075$), and QDAF circularity ($\chi^2(1) = 0.009$, $P = 0.927$). Even the interreader agreement was not different between GAF- and BAF-based grading and in the same range as the overall results presented above: DDAF lesion size (ICC: GAF, 0.996; BAF, 0.997), QDAF lesion size (ICC: GAF, 0.980; BAF, 0.977), DDAF perimeter (ICC: GAF, 0.996; BAF, 0.997), QDAF perimeter (ICC: GAF, 0.964; BAF, 0.966), DDAF circularity (ICC: GAF, 0.980; BAF, 0.975), and QDAF circularity (ICC: GAF, 0.950; BAF, 0.885). Of note, RPE atrophy was evaluated as foveal noninvolving in the same 21 eyes (GAF and BAF) by all five independent readers with total congruency, suggesting less influence of macular pigment on BAF images in *ABCA4*-related retinopathy.

Discussion

To our knowledge, this is the first study that systematically investigated interreader and intermodality agreement for semiautomated grading of RPE atrophy lesion size, perimeter, and circularity secondary to *ABCA4*-related retinopathy using GAF and BAF imaging. Both GAF and BAF imaging were demonstrated to allow for reproducible area measurements of RPE atrophy. GAF-based quantification revealed slightly albeit not significantly higher interreader agreement. Hence, not only conventional BAF-based, but also the innovative GAF-based grading may be suitable as a tool for progression assessment (i.e., clinical endpoint) in *ABCA4*-related retinopathy.

In contrast to our results, recent studies described significant differences between GAF and BAF-based measurements of GA secondary to AMD, most pronounced in eyes with foveal noninvolvement.[17,25]

Various possible explanations may be considered. Firstly, previous publications using quantitative AF demonstrated that *ABCA4*-related retinopathy exhibits high AF intensity,[10–12] while AMD exhibits rather low AF levels.[45] Thus, central shadowing of BAF-images due to macular pigment may be less pronounced in *ABCA4*-related retinopathy (Figs. 1, 3). Therefore, grading of foveal involvement of RPE atrophy secondary to *ABCA4*-related retinopathy was very congruent in our cohort. In contrast to those AMD studies, eyes with foveal noninvolvement also showed excellent interreader agreement of BAF-based measurements in our cohort, leading to more congruent results between both AF modalities in our study. Of note, very mild phenotypes with less elevated AF levels might potentially be more affected by blue light absorption due to macular pigment as can be seen in one example of Figure 3.[11] In these cases, very early and faint changes, such as granular appearance and/or hypoautofluorescence, might theoretically be slightly better detectable with GAF imaging. Secondly, "shadow correction" and the possibility of manual constraints in the newer RegionFinder software may account for enhanced grading. Thirdly, optic media opacities (i.e., cataract or vitreous floaters) have been described to reduce the transmission of short-wavelength light possibly leading to less sharp lesion boundaries in BAF compared to GAF.[46] Of note, our subjects were on average younger compared to the published AMD cohorts, which may have caused increased image quality due to lower prevalence of media opacities. Fourthly, before GAF and BAF images are acquired, the focus usually is adjusted in the infrared-reflection (IR) mode. Whenever switching to GAF or BAF, the focus has to be readjusted due to chromatic aberrations. In contrast to both AMD studies, we used the simultaneous GAF and BAF mode that compensated for this source of error between BAF and GAF images as the focus should be set to enable sharp images of both AF modalities. Thus, evaluation of our acquired GAF and BAF image quality did not reveal any noticeable difference in sharpness (Figs. 1, 3).

For *ABCA4*-related retinopathy, it has been speculated that BAF imaging may induce apoptosis in RPE cells in the presence of excessive accumulation of lipofuscin as observed in *Abca4*-knockout mice and cell cultures, respectively.[27,28,47–52] However, there is no evidence of phototoxic effects in humans. Nevertheless, reduced-illuminance AF imaging (RAFI) has been proposed to reduce the high-energetic light exposure and potentially associated adverse effects.[29] An adaption of the RAFI mode is recently examined in *ABCA4*-related retinopathy by the multicenter ProgStar study.[30] Of note, in a small study cohort BAF and RAFI were reported to show distinct variability in the assessment of QDAF.[53] Ex vivo experiments with cultured human RPE cells demonstrated that illumination with less-energetic green light shows substantially fewer to no nonviable cells as compared to illumination with blue light where a dependence on exposure duration and A2E concentration was found.[27,48] Therefore, GAF imaging may represent an alternative, given that it is theoretically implementable in most cSLO devices (e.g., Heidelberg Engineering Spectralis HRA with MultiColor imaging). Furthermore, GAF is more patient friendly and comfortable due to less blinding (anecdotal evidence as described by each of our subject),[17] giving an additional benefit concerning imaging compliance in study environment and/or clinical workup.

Clinical endpoints are inevitable for upcoming therapeutic trials. RPE atrophy assessed by GAF or BAF imaging as morphologic surrogate marker for *ABCA4*-related retinopathy harbors great potentials but also constitutes difficult challenges: (1) RPE atrophy secondary to *ABCA4*-related retinopathy presents in a variable manner from irregular hypoautofluorescent pattern to well-demarcated uniform hypoautofluorescent areas. Indeed, some studies suggested that QDAF may be considered as a transition state between normal retina and DDAF.[22,36] DDAF and QDAF should therefore be evaluated separately in order to avoid misinterpretations.[20,30,36] (2) Subjective determinations of the semiautomated grading bias the results the more widespread and less demarcated the lesions are. Hence, QDAF revealed distinctly higher intermodality as well as interreader variation compared to DDAF. The different presentation of DDAF and especially QDAF (i.e., most widespread and multifocal in group 3) might therefore also account for differences in the three ERG-based groups. Furthermore, the subjective determination mostly affects the last (i.e., most eccentric) pixels of each lesion, explaining why both shape-descriptive factors showed consistently less reliable results compared to lesion size measurement. This may implicate DDAF lesion size to be the most accurate available morphologic surrogate marker in *ABCA4*-related retinopathy to date. (3) Ideal clinical endpoints should assess disease progression prior to irreversible changes, because treatment-effects may not be observable otherwise. However, the presence of RPE atrophy signified the

focal end-stage of *ABCA4*-related retinopathy disease progression. As it is thought to occur after the hitherto unknown point-of no return, changes within the area of atrophy might be functionally relevant. Progression rates and treatment effects might therefore be assessed by alterations in the surrounding area including expansion of RPE atrophy. In the knowledge of slower progression rates of RPE-atrophy in *ABCA4*-related retinopathy compared to other retinal degenerations like AMD,[15,18,19] lowest grading variations should be aspired in order to correctly assess true growth. Depending on our results, we might therefore recommend the use of DDAF in GAF imaging. However, there were no significant differences in interreader agreement compared to BAF-related grading. Other imaging tools like quantitative AF visualize earlier pathognomonic alterations (i.e., lipofuscin accumulation).[10–12] However, the potential as clinical endpoint cannot finally be evaluated as longitudinal data are still pending. (4) Since there are inconsistent reports concerning the correlation of deep scotomata and the boundaries of RPE atrophy secondary to *ABCA4*-related retinopathy,[54–57] more data are still needed. Large prospective multicenter studies like ProgStar may provide the necessary assurances that progression of atrophy can be accepted as an anatomic endpoint to gauge the functional relevant effects of future treatments.[30]

Intermodality and interreader variability was limited in presence of very large lesions by the image frame (30° × 30°) defining the maximum measurable lesion extent. Using wide-field imaging, the intermodality and interreader variability for large lesions may therefore possibly be larger. This might especially affect group 3 eyes as well as QDAF lesions as they usually are more widespread and eccentric. Further, we did not obtain OCT imaging, which may be the most common imaging modality besides AF approaching RPE atrophy (hypertransmission into choroid). Yet, previous studies reported that the agreement of RPE atrophy secondary to AMD was better for BAF than OCT, most likely due to hyposcattering of large choroidal vessels that lead to segmentation artefacts.[58] Still, future studies on innovative technics such as swept-source OCT devices or adaptive optics are of interest and merit further investigations.[59,60] Small study cohorts are common as *ABCA4*-related retinopathy ranks among the rare retinal diseases. Nevertheless, this is the overall largest study to provide a systematic investigation of the interreader and intermodality agreement for semi-automated grading of RPE atrophy using GAF and BAF imaging to date.

In conclusion, in this study GAF- and BAF-based quantification of RPE atrophy secondary *ABCA4*-related retinopathy was proven to be reliable. The high interreader agreement may especially validate DDAF lesion size as clinical endpoint for future interventional clinical trials. Both AF modalities showed comparable results, suggesting a possible advantage of GAF in terms of less energetic excitation light.

Acknowledgments

None of the authors has a proprietary interest. This work was supported by the ProRetina Deutschland, Aachen, Germany; the Association of Rhine-Westphalian Ophthalmologists (RWA), Recklinghausen, Germany; the BONFOR research program of the University of Bonn, Bonn, Germany (Grant No O-137.0023 to PLM and O-137.0022 to MP); and the German Research Foundation (DFG; Grant MU4279/1-1 to PLM, FL 658/4-1 as well as FL 658/4-2 to MF and Ho1926/3-1 to FGH). No sponsor or funding agency had any involvement in the design, collection, analysis, and interpretation of the data; manuscript writing; and the decision to submit the manuscript for publication.

Disclosure: **P.L. Müller,** Heidelberg Engineering (F), Optos (F), Carl Zeiss MedicTec (F), CenterVue (F); **M. Pfau,** Heidelberg Engineering (F), Optos (F), Carl Zeiss MedicTec (F), CenterVue (F); **M.M. Mauschitz,** Heidelberg Engineering (F), Optos (F), Carl Zeiss MedicTec (F), CenterVue (F); **P.T. Möller,** Heidelberg Engineering (F), Optos (F), Carl Zeiss MedicTec (F), CenterVue (F); **J. Birtel,** Heidelberg Engineering (F), Optos (F), Carl Zeiss MedicTec (F), CenterVue (F); **P. Chang,** Heidelberg Engineering (F), Optos (F), Carl Zeiss MedicTec (F), CenterVue (F); **M. Gliem,** Heidelberg Engineering (F), Optos (F), Carl Zeiss MedicTec (F), CenterVue (F); **S. Schmitz-Valckenberg,** Heidelberg Engineering (F), Optos (F), Carl Zeiss MedicTec (F, R), CenterVue (F), Allergan (F, R), Alcon/Novartis (C, F, R), Bioeq/Fermycon (F, C), Genentech/Roche (F, R), Bayer (F, R); **M. Fleckenstein,** Heidelberg Engineering (F, R), Optos (F), Carl Zeiss MedicTec (F), CenterVue (F), Alcon/Novartis (F, R), Bayer (F, R), Roche (C, F, R); Pending patent: US20140303013 A1 (P); **F.G. Holz,** Heidelberg Engineering (F, C, R), Optos (F), Carl Zeiss MedicTec (F, C), CenterVue (F), Allergan (F,

R), Alcon/Novartis (F, R), Genentech/Roche (F, R), Bayer (F, R), Acucela (F, R), Boehringer Ingelheim (F, R); **P. Herrmann,** Heidelberg Engineering (F), Optos (F), Carl Zeiss MedicTec (F), CenterVue (F)

References

1. Hamel CP. Cone rod dystrophies. *Orphanet J Rare Dis*. 2007;2:7.
2. Kitiratschky VBD, Grau T, Bernd A, et al. ABCA4 gene analysis in patients with autosomal recessive cone and cone rod dystrophies. *Eur J Hum Genet*. 2008;16:812–819.
3. Riveiro-Alvarez R, Lopez-Martinez M-A, Zernant J, et al. Outcome of ABCA4 disease-associated alleles in autosomal recessive retinal dystrophies: retrospective analysis in 420 Spanish families. *Ophthalmology*. 2013;120:2332–2337.
4. Birtel J, Eisenberger T, Gliem M, et al. Clinical and genetic characteristics of 251 consecutive patients with macular and cone/cone-rod dystrophy. *Sci Rep*. 2018;8:4824.
5. Allikmets R, Singh N, Sun H, et al. A photoreceptor cell-specific ATP-binding transporter gene (ABCR) is mutated in recessive Stargardt macular dystrophy. *Nat Genet*. 1997;15:236–246.
6. Koenekoop RK. The gene for Stargardt disease, ABCA4, is a major retinal gene: a mini-review. *Ophthalmic Genet*. 2003;24:75–80. Available at: http://www.ncbi.nlm.nih.gov/pubmed/12789571. Accessed July 23, 2014.
7. Mata NL, Weng J, Travis GH. Biosynthesis of a major lipofuscin fluorophore in mice and humans with ABCR-mediated retinal and macular degeneration. *Proc Natl Acad Sci U S A*. 2000;97:7154–7159.
8. Delori FC, Staurenghi G, Arend O, Dorey CK, Goger DG, Weiter JJ. In vivo measurement of lipofuscin in Stargardt's disease—Fundus flavimaculatus. *Invest Ophthalmol Vis Sci*. 1995;36:2327–2331. Available at: http://www.ncbi.nlm.nih.gov/pubmed/7558729. Accessed September 18, 2014.
9. Delori FC, Dorey CK, Staurenghi G, Arend O, Goger DG, Weiter JJ. In vivo fluorescence of the ocular fundus exhibits retinal pigment epithelium lipofuscin characteristics. *Invest Ophthalmol Vis Sci*. 1995;36:718–729. Available at: http://www.ncbi.nlm.nih.gov/pubmed/7890502. Accessed September 18, 2014.
10. Cideciyan AV, Aleman TS, Swider M, et al. Mutations in ABCA4 result in accumulation of lipofuscin before slowing of the retinoid cycle: a reappraisal of the human disease sequence. *Hum Mol Genet*. 2004;13:525–534.
11. Burke TR, Duncker T, Woods RL, et al. Quantitative fundus autofluorescence in recessive Stargardt disease. *Invest Ophthalmol Vis Sci*. 2014;55:2841–2852.
12. Müller PL, Gliem M, Mangold E, et al. Monoallelic ABCA4 mutations appear insufficient to cause retinopathy: a quantitative autofluorescence study. *Invest Opthalmol Vis Sci*. 2015;56:8179.
13. Deckert A, Schmitz-Valckenberg S, Jorzik J, Bindewald A, Holz FG, Mansmann U. Automated analysis of digital fundus autofluorescence images of geographic atrophy in advanced age-related macular degeneration using confocal scanning laser ophthalmoscopy (cSLO). *BMC Ophthalmol*. 2005;5:1.
14. Schmitz-Valckenberg S, Brinkmann CK, Alten F, et al. Semiautomated image processing method for identification and quantification of geographic atrophy in age-related macular degeneration. *Invest Ophthalmol Vis Sci*. 2011;52:7640–7646.
15. Lambertus S, Lindner M, Bax NM, et al. Progression of late-onset Stargardt disease. *Invest Opthalmol Vis Sci*. 2016;57:5186.
16. Csaky KG, Richman EA, Ferris FL. Report from the NEI/FDA Ophthalmic Clinical Trial Design and Endpoints Symposium. *Invest Ophthalmol Vis Sci*. 2008;49:479–489.
17. Pfau M, Goerdt L, Schmitz-Valckenberg S, et al. Green-light autofluorescence versus combined blue-light autofluorescence and near-infrared reflectance imaging in geographic atrophy secondary to age-related macular degeneration. *Invest Opthalmol Vis Sci*. 2017;58:121–130.
18. McBain VA, Townend J, Lois N. Progression of retinal pigment epithelial atrophy in stargardt disease. *Am J Ophthalmol*. 2012;154:146–154.
19. Lindner M, Lambertus S, Mauschitz MM, et al. Differential disease progression in atrophic age-related macular degeneration and late-onset Stargardt disease. *Invest Opthalmol Vis Sci*. 2017;58:1001.
20. Kuehlewein L, Hariri AH, Ho A, et al. Comparison of manual and semiautomated fundus autofluorescence analysis of macular atrophy in Stargardt disease phenotype. *Retina*. 2016;36:1216–1221.
21. Lambertus S, Bax NM, Fakin A, et al. Highly sensitive measurements of disease progression in

rare disorders: developing and validating a multimodal model of retinal degeneration in Stargardt disease. Wedrich A, ed. *PLoS One*. 2017;12:e0174020.
22. Ho A, Kuehlewein L, Hariri A, et al. Quantitative characteristics of spectral-domain optical coherence tomography (SDOCT) in corresponding areas of decreased autofluorescence in patients with Stargardt disease. *Invest Opthalmol Vis Sci*. 2015;56:5924.
23. Lindner M, Böker A, Mauschitz MM, et al. Directional kinetics of geographic atrophy progression in age-related macular degeneration with foveal sparing. *Ophthalmology*. 2015;122:1356–1365.
24. Delori FC, Goger DG, Hammond BR, Snodderly DM, Burns SA. Macular pigment density measured by autofluorescence spectrometry: comparison with reflectometry and heterochromatic flicker photometry. *J Opt Soc Am A Opt Image Sci Vis*. 2001;18:1212–1230. Available at: http://www.ncbi.nlm.nih.gov/pubmed/11393613. Accessed April 28, 2015.
25. Wolf-Schnurrbusch UE, Wittwer VV, Ghanem R, et al. Blue light versus green light autofluorescence: lesion size of areas with geographic atrophy. *Invest Ophthalmol Vis Sci*. 2011;52:9497–9502.
26. Müller PL, Müller S, Gliem M, et al. Perception of Haidinger brushes in macular disease depends on macular pigment density and visual acuity. *Invest Ophthalmol Vis Sci*. 2016;57:1448–1456.
27. Sparrow JR, Nakanishi K, Parish CA. The lipofuscin fluorophore A2E mediates blue light-induced damage to retinal pigmented epithelial cells. *Invest Ophthalmol Vis Sci*. 2000;41:1981–1989. Available at: http://www.ncbi.nlm.nih.gov/pubmed/10845625. Accessed July 24, 2014.
28. Teussink MM, Lambertus S, de Mul FF, et al. Lipofuscin-associated photo-oxidative stress during fundus autofluorescence imaging. Lewin AS, ed. *PLoS One*. 2017;12:e0172635.
29. Cideciyan AV, Swider M, Aleman TS, et al. Reduced-illuminance autofluorescence imaging in ABCA4-associated retinal degenerations. *J Opt Soc Am A Opt Image Sci Vis*. 2007;24:1457–1467. Available at: http://www.pubmedcentral.nih.gov/articlerender.fcgi?artid=2579898&tool=pmcentrez&rendertype=abstract. Accessed July 28, 2014.
30. Strauss RW, Ho A, Muñoz B, et al. The natural history of the progression of atrophy secondary to Stargardt disease (ProgStar) studies. *Ophthalmology*. 2016;123:817–828.
31. Charbel Issa P, Barnard AR, Herrmann P, Washington I, MacLaren RE. Rescue of the Stargardt phenotype in Abca4 knockout mice through inhibition of vitamin A dimerization. *Proc Natl Acad Sci*. 2015;112:8415–8420.
32. Schwartz SD, Hubschman J-P, Heilwell G, et al. Embryonic stem cell trials for macular degeneration: a preliminary report. *Lancet*. 2012;379:713–720.
33. Han Z, Conley SM, Naash MI. Gene therapy for Stargardt disease associated with ABCA4 gene. *Adv Exp Med Biol*. 2014;801:719–724.
34. Eisenberger T, Neuhaus C, Khan AO, et al. Increasing the yield in targeted next-generation sequencing by implicating CNV analysis, non-coding exons and the overall variant load: the example of retinal dystrophies. *PLoS One*. 2013;8:e78496.
35. Fujinami K, Lois N, Mukherjee R, et al. A longitudinal study of Stargardt disease: quantitative assessment of fundus autofluorescence, progression, and genotype correlations. *Invest Ophthalmol Vis Sci*. 2013;54:8181–8190.
36. Strauss RW, Muñoz B, Ho A, et al. Incidence of atrophic lesions in Stargardt disease in the Progression of Atrophy Secondary to Stargardt Disease (ProgStar) Study. *JAMA Ophthalmol*. 2017;53:841–852.
37. Domalpally A, Danis RP, White J, et al. Circularity index as a risk factor for progression of geographic atrophy. *Ophthalmology*. 2013;120:2666–2671.
38. Lois N, Holder GE, Bunce C, Fitzke FW, Bird AC. Phenotypic subtypes of Stargardt macular dystrophy-fundus flavimaculatus. *Arch Ophthalmol*. 2001;119:359–369. Available at: http://www.ncbi.nlm.nih.gov/pubmed/11231769. Accessed July 23, 2014.
39. Zahid S, Jayasundera T, Rhoades W, et al. Clinical phenotypes and prognostic full-field electroretinographic findings in Stargardt disease. *Am J Ophthalmol*. 2013;155:465–473.e3.
40. R Development Core Team. R: A language and environment for statistical computing. Vienna, Austria: R Foundation for Statistical Computing. 2015. Available at: https://www.r-project.org/.
41. Feuer W, Yehoshua Z, Gregori G, Al E. Square root transformation of geographic atrophy area measurements to eliminate dependence of growth rates on baseline lesion measurements: a reanalysis of age-related eye disease study report no. 26. *JAMA Ophthalmol*. 2013;131:110–111.
42. Yehoshua Z, Rosenfeld PJ, Gregori G, et al. Progression of geographic atrophy in age-related

macular degeneration imaged with spectral domain optical coherence tomography. *Ophthalmology*. 2011;118:679–686.
43. Shrout PE, Fleiss JL. Intraclass correlations: uses in assessing rater reliability. *Psychol Bull*. 1979; 86:420–428.
44. Bland JM, Altman D. Statistical methods for assessing agreement between two methods of clinical measurement. *Lancet*. 1986;327:307–310.
45. Gliem M, Müller PL, Finger RP, McGuinness M, Holz FG, Charbel Issa P. Quantitative fundus autofluorescence in early and intermediate age-related macular degeneration. *JAMA Ophthalmology*. 2016;134(7):817–824.
46. Boettner EA, Wolter JR. Transmission of the ocular media. *Invest Ophthalmol Vis Sci*. 1962;1: 776–783.
47. Weng J, Mata NL, Azarian SM, Tzekov RT, Birch DG, Travis GH. Insights into the function of Rim protein in photoreceptors and etiology of Stargardt's disease from the phenotype in abcr knockout mice. *Cell*. 1999;98:13–23.
48. Dorey CK, Delori FC, Akeo K. Growth of cultured RPE and endothelial cells is inhibited by blue light but not green or red light. *Curr Eye Res*. 1990;9:549–559. Available at: http://www.ncbi.nlm.nih.gov/pubmed/2117518. Accessed December 18, 2017.
49. Wihlmark U, Wrigstad A, Roberg K, Nilsson SE, Brunk UT. Lipofuscin accumulation in cultured retinal pigment epithelial cells causes enhanced sensitivity to blue light irradiation. *Free Radic Biol Med*. 1997;22:1229–1234. Available at: http://www.ncbi.nlm.nih.gov/pubmed/9098097. Accessed December 18, 2017.
50. Crockett RS, Lawwill T. Oxygen dependence of damage by 435 nm light in cultured retinal epithelium. *Curr Eye Res*. 1984;3:209–215. Available at: http://www.ncbi.nlm.nih.gov/pubmed/6690222. Accessed December 18, 2017.
51. Putting BJ, Van Best JA, Vrensen GF, Oosterhuis JA. Blue-light-induced dysfunction of the blood-retinal barrier at the pigment epithelium in albino versus pigmented rabbits. *Exp Eye Res*. 1994;58: 31–40.
52. Hafezi F, Marti A, Munz K, Remé CE. Light-induced apoptosis: differential timing in the retina and pigment epithelium. *Exp Eye Res*. 1997;64: 963–970.
53. Strauss RW, Muñoz B, Jha A, et al. Comparison of short-wavelength reduced-illuminance and conventional autofluorescence imaging in Stargardt macular dystrophy. *Am J Ophthalmol*. 2016;168:269–278.
54. Sunness JS. What you see is not always what you get in atrophic macular disease. *Retin Cases Brief Rep*. 2008;2:205–208.
55. Bernstein A, Sunness JS, Applegate CA, Tegins EO. Mapping the dense scotoma and its enlargement in Stargardt disease. *Retina*. 2016;36:1741–1750.
56. Sunness JS, Steiner JN. Retinal function and loss of autofluorescence in Stargardt disease. *Retina*. 2008;28:794–800.
57. Cideciyan AV, Swider M, Aleman TS, et al. Macular function in macular degenerations: repeatability of microperimetry as a potential outcome measure for ABCA4-associated retinopathy trials. *Invest Ophthalmol Vis Sci*. 2012;53: 841–852.
58. Hu Z, Medioni GG, Hernandez M, Hariri A, Wu X, Sadda SR. Segmentation of the geographic atrophy in spectral-domain optical coherence tomography and fundus autofluorescence images. *Invest Ophthalmol Vis Sci*. 2013;54:8375–8383.
59. Domdei N, Reiniger JL, Pfau M, Charbel Issa P, Holz FG, Harmening WM. Histologie im lebenden Auge. *Der Ophthalmol*. 2017;114:206–214.
60. Reiniger J, Domdei N, Pfau M, Müller PL, Holz F, Harmening W. Adaptive Optiken – Möglichkeiten für die Diagnostik hereditärer Netzhauterkrankungen. *Klin Monbl Augenheilkd*. 2017;234:311–319.